



The dry-to-wet transition of fiber networks-Return to mechanical stability

Downloaded from: <https://research.chalmers.se>, 2025-12-05 01:46 UTC

Citation for the original published paper (version of record):



Bergström, P., Hanson, C., Ström, H. et al (2023). The dry-to-wet transition of fiber networks-Return to mechanical stability. AICHE Journal, 69(9). <http://dx.doi.org/10.1002/aic.18148>

N.B. When citing this work, cite the original published paper.

RESEARCH ARTICLE

Particle Technology and Fluidization

The dry-to-wet transition of fiber networks—Return to mechanical stability

Per Bergström^{1,2}  | Charlotta Hanson^{2,3} | Henrik Ström¹  | Srdjan Sasic¹¹Department of Mechanics and Maritime Sciences, Division of Fluid Dynamics, Chalmers University of Technology, Gothenburg, Sweden²Essity Hygiene and Health AB, Mölndal, Sweden³Department of Chemistry and Chemical Engineering, Chalmers University of Technology, Gothenburg, Sweden

Correspondence

Per Bergström, Department of Mechanics and Maritime Sciences, Division of Fluid Dynamics, Chalmers University of Technology, Gothenburg, Sweden.

Email: pellebergstrom@gmail.com

Abstract

In this article, we provide a comprehensive experimental, numerical, and theoretical explanation of the dry-to-wet transition of nonbonded fiber networks made of natural fibers. Given that the main functionality of many common products consisting of fluff pulp fiber networks requires absorption of liquids, we focus on understanding the solid volume fraction transition from a dry to a wet state as a crucial component for controlling properties such as permeability and capillary pressure, on which product function eventually depends. From studying the wetting of fluff pulp fiber networks with a distribution of fiber lengths, we show that the change in the solid volume fraction going from dry to wet state is driven by the disappearance of fiber-fiber adhesion. The mechanically stable state to which the network transitions is independent of its prior dry solid volume fraction and predetermined primarily by the fiber aspect ratio.

KEYWORDS

fibers, mechanics, particle technology, porous media

1 | INTRODUCTION

Fiber networks are commonly seen in both man-made materials (e.g., paper, hygiene products, and nonwoven) and biological materials (e.g., collagen fiber networks and cytoskeleton of eukaryotic cells). Fiber networks are often used industrially and encountered in the biological world for their mechanical properties in relation to weight, as well as their fluid transport properties due to the inherent permeable nature of these materials. The packing density of the network is often characterized by the bulk density, or as we choose in this article, the closely related solid volume fraction (SVF) defined as the ratio of solid material volume to total volume. These characteristics have a strong influence on mechanical and fluid transport properties of the networks, such as tensile strength, softness, capillary pressure, and permeability. This influence is often used in both nature and industry to tailor materials with specific properties. However, due to the in many

cases extreme softness or deformability of this type of networks, even the smallest stress on the networks can have a significant impact on the SVF of the material and, consequently, on both the mechanical behavior and the fluid transport properties of the network. This leads to a great importance of understanding network deformation and its impact on the network SVF.

For nonbonded semi-flexible fiber networks much work has been done in literature related to the relationship between compressive stress and network deformation as well as network configuration, such as changes in the network SVF and the average number of fiber-fiber contacts per fiber in the structure. In this article, we have chosen to use the term pressure for compressive stress and will do so henceforth.

Studying compression of fiber networks, van Wyk developed a semi-empirical model for pressure as a function of density, based on statistics of contact formation and the scaling laws of bending beams.¹

This is an open access article under the terms of the [Creative Commons Attribution](https://creativecommons.org/licenses/by/4.0/) License, which permits use, distribution and reproduction in any medium, provided the original work is properly cited.

© 2023 The Authors. *AIChE Journal* published by Wiley Periodicals LLC on behalf of American Institute of Chemical Engineers.

In his equation, the pressure is dependent on the network density, the unloaded network density, a factor being dependent on, among other factors, fiber stiffness and an exponent being predominantly dependent on fiber orientation.

The work by van Wyk was followed by a further development of statistical models for average number of fiber-fiber contacts in relation to SVF by Komori and Makishima, later extended by Toll.^{2,3} Further, theoretical considerations were provided by Evans and Gibson, extended by Toll and Wouterse et al., explaining the maximum degree of packing of rigid rods.^{3–5} This was done by combining the theories for number of fiber-fiber contacts as a function of the SVF with those related to the concept of *caging number*, the latter being defined as the average minimum number of randomly placed fiber-fiber contacts on a single fiber that immobilize all its translations and rotations.

Further studies on mechanics of fiber networks include numerical studies of nonbonded fiber networks primarily using discrete element (DEM) or bead-spring models to capture fiber deformation and also to account for fiber-fiber rearrangement (see Section S1 in the Supporting Information).

In our previous work, we have used DEM to identify the phenomena behind the change in the SVF due to uniaxial compression of nonbonded fluff pulp fiber networks in a dry state.⁶ It was found that the experimentally observed nonreversible deformation could be explained by fiber-fiber adhesion which is suggested to be stemming from moisture, with the nonreversible deformation at high degrees of compression being amplified by plastic deformation in the fiber-fiber contact points effectively increasing the effect of the adhesion.

In this work, we will investigate the change in the SVF for natural nonbonded fluff pulp networks with an inherent distribution in fiber length when going from a dry to a wet state. Such changes in the network SVF in fluff pulp fiber networks have been observed experimentally in literature.⁷ Changes can be expected due to the change in fiber properties of cellulose fibers when going from a dry to a wet state, including fiber elastic modulus and swelling of the fiber cross sectional area.⁸ Interactions between fibers can also be expected to change in the wet state due to the moisture sensitivity of fiber-fiber adhesion which affects the network structure in the dry state.

In the present study, we will in the first stage use experiments to characterize and quantify the change in the network structure of nonbonded fluff pulp fiber networks of varying SVFs when transitioning from a dry to a wet state. In the second stage, we will compare experimental results with those obtained by our DEM simulations and identify the main physics behind the observed changes to the network SVF due to the transition. Finally, in the third stage, we will utilize results from the simulations in combination with theoretical considerations by other research groups to provide a comprehensive theoretical explanation regarding the network state to which the wet network transitions.

2 | MEASUREMENTS

We performed measurements to look at the behavior of the SVF of fiber networks when going from a dry to a completely wet state. The

networks tested consisted of air-laid Southern Pine pulp fibers compressed to a varying degree by dry uniaxial compression in order to create networks with a varying dry SVF.

Based on the previously shown results from literature, the micro-mechanics and SVF of this type of materials are known to be highly dependent on pressure, placing emphasis on the conditions under which the measuring of SVF is performed. In this study, we choose to primarily focus on characterizing the change in the SVF of a network in the unloaded state. We will use here the term *Base Case* for the measurements performed in an unloaded state.

To complement the measurement procedure, we have decided to use two additional approaches (termed hereafter *Case II* and *Case III*) to measure the SVF after transitioning from dry to wet state. For *Case II*, we use the more commonly used approach of measuring thickness of this type of materials, which is under a slight pressure.⁹ Finally, for *Case III*, we measure the SVF in a fully saturated state but not submerged in water, which will lead to the network being subjected to slight pressure stemming from the wet weight of the material and the capillary forces. For an extensive description of the experimental method and material, we refer to Section S2 in the Supporting Information.

2.1 | Experimental results and discussion

We present in Figure 1 the results from measurements of the wet SVFs with a varying dry SVF for *Base Case*, *Case II*, and *Case III*. A table summarizing the three experimental procedures can be found in Table S1.

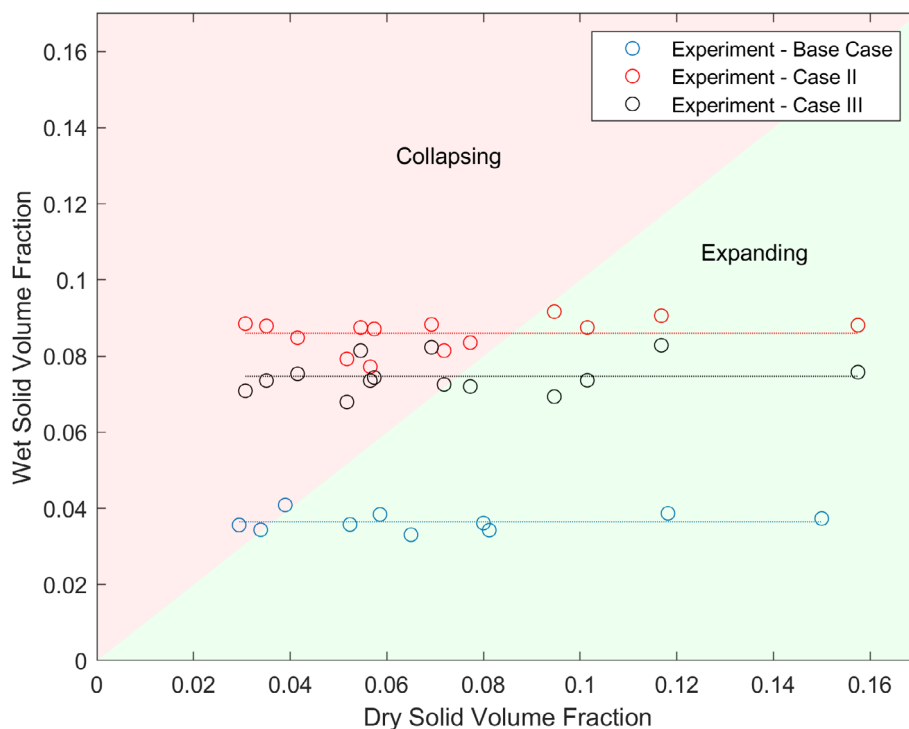
The experimental results show the resulting wet SVF being independent of the initial dry solid volume fraction. The tending of the wet solid volume fraction to a close to the same value is seen in all three measurement procedures, *Base Case* (submerged and unloaded), *Case II* (submerged under 0.45 kPa load), and *Case III* (fully saturated and unloaded). The average values of the wet solid volume fraction, however, are shown to be very sensitive to the different loading cases in the wet state. *Base Case* exhibits an average wet solid volume fraction of 0.036, *Case II* yields an average of 0.086, and *Case III* has an average of 0.075. Our observed trend of wet solid volume fraction tending to the same value is also seen in Buchholz et al., in which the authors used a method similar to that in *Case II* as reference measurements when studying mixture of pulp and superabsorbent particles.⁷

The obtained results allow us to draw three important conclusions:

1. The state to which the network transitions when going from a dry to a wet state is independent of its prior dry solid volume fraction.

We have shown that for each case all samples end up at close to the same wet solid volume fraction, albeit with different values for the three cases measured. This indicates that the process of going from a dry to a wet state, for the networks tested having the same fiber composition but with widely differing solid volume fractions due

FIGURE 1 Experimental results and mean values of the networks in our work transitioning from dry to wet state, measured with Base Case (blue), Case II (red), and Case III (black). The top left region (light red) signifies an increase of the SVF (collapse of the network on a micro-level) when going from a dry to a wet state. The bottom right region (light green) indicates a decrease of the SVF (expansion of the network on a micro-level) when going from a dry to a wet state. A consistent trend of the resulting wet SVF being independent of the dry SVF is observed in all three cases. The resulting level of the wet SVF, however, is proven very sensitive to the different loading cases in the wet state.



to varying prior compression, transitions the networks to the same wet state with the same network configuration. The only difference between the three cases being the load applied to the network in each different experimental case.

2. The level of solid volume fraction of networks in the wet state is extremely sensitive to the degree of loading of the network.

The differences in the average wet solid volume fraction between the three cases measured here are explained by the extreme deformability of the material. *Case II* wet solid volume fraction is increased compared to that in the unloaded state in *Base Case* due to the applied external load of 0.45 kPa. On the other hand, the *Case III* wet solid volume fraction is increased compared to that in *Base Case* due to compaction of the network from its own wet weight in combination with capillary forces.

3. No fiber or network parameter that affects final packing of the wet sample has been affected by the compression of the network or the effect is annulled by the presence of water.

The shown reversion of networks with widely varying dry solid volume fractions to a single one and with the same network configuration when transitioned to the wet state brings important information regarding the source of nonreversible deformation sustained from the compression used to create networks of a varying dry solid volume fraction. The fact that for all three cases, both networks that have been compressed to a high degree and the uncompressed networks end up at the same wet solid volume fraction, either by expanding or collapsing, allows us to conclude that no fiber or

network parameter that affects final packing of the wet samples has been affected by the compression of the network or the effect is annulled by the presence of water. In our previous work, we suggested the source of nonreversible deformation from dry compression to be a synergetic effect of inter-fiber adhesion and plastic deformation in fiber-fiber contact points.⁶ The results from the measurements in the present study (Figure 1) seem to further corroborate this assumption, indicating that the fiber-fiber adhesion in the dry state is annulled in the wet state supporting the suggested source of the inter-fiber adhesion to be due to moisture. Further, if plastic deformation of fibers either in the form of plastic bending deformation or plastic contact deformation plays a role, the effect is either very local, acting only to amplify the effect of adhesion, or small enough not to affect the final packing of the wet sample.

While the experimental results bring important conclusions regarding the spontaneous network deformation due to the transition from dry to wet state, a number of open questions remain:

- Can the physics behind the change in the network solid volume fraction from dry to wet state be explained as driven mainly by the disappearance of fiber-fiber adhesion in combination with changes in fiber mechanical properties when wet?
- What is the nature of the state to which the wet network is tending and what are the main network and fiber parameters influencing the level of solid volume fraction in the wet state?

To answer these questions, we will model fiber networks based on the assumption that nonreversible deformation in the dry state is driven mainly by fiber-fiber adhesion stemming from moisture and that this inter-fiber adhesion disappears in the wet state. We will then

simulate the transition from dry to wet state for networks with varying dry solid volume fractions and compare to experiments in order to test our assumptions.

3 | NUMERICAL FRAMEWORK

Modeling of fiber networks in this work has been done using Discrete Element Modeling (DEM). DEM is based on the conservation of linear momentum and angular momentum of particles. The modeling is done on a fiber-level where each individual fiber is represented by a string of interacting spherical particles. This method is frequently used in literature (see Section S1 in the Supporting Information), and is commonly referred to as a bead-spring model. Particle interactions can take various forms, such as contact interactions in the normal direction, compressibility of particles, or adhesion between particles and tangential direction through inter-particle friction. Particles may also be bonded together and interact through forces or torques between the bonded particles. These particle-particle bonds are used to connect a string of particles in order to represent a fiber and preserve its integrity.

In this work, we are using the open source DEM software LIGGGHTS with particle-particle bonds based on the work by Richter and Schramm et al.^{10–12} This results in a representation of fibers that facilitates translation, rotation, and relative sliding of fibers, while at the same time capturing fiber geometry, mechanical properties, and contact interactions of fibers. Detailed descriptions regarding modeling of fibers in dry and wet state, network generation and simulation procedure for the transition of the network from dry to wet state can be found in Section S3 of the Supporting Information.

3.1 | Simulation results and discussion

We have done the simulations primarily to answer the questions still remaining after the analysis of our experimental results. The questions are predominantly related to identification of the fundamental phenomena that lead to the change in the network solid volume fraction when a network transitions from a dry to a wet state and to an understanding of the phenomena behind the state to which the networks is tending. To do so, we set up a simulation procedure that starts from a network with dry properties, changes the network to having wet properties and then let the network settle to a new mechanical equilibrium state. Typically, this involves the network either expanding or collapsing due to changes in the fiber properties and fiber-fiber interactions. We note that we are not interested in looking at the transient phase of the transition but rather in the equilibrium states.

We hypothesize that in the dry state the fiber-fiber adhesion prevents low solid volume fraction networks from compacting due to gravity to a higher solid volume fraction packing. The effect is similar to the effect of high fiber-fiber friction preventing networks from compacting to a denser network. For high solid volume fraction networks, the same adhesion is what prevents fibers from reverting back

to a relaxed state and the network to expand to a lower solid volume fraction packing. In the wet state, adhesion disappears and both high- and low-solid volume fraction networks are tending to the same value of the solid volume fraction.

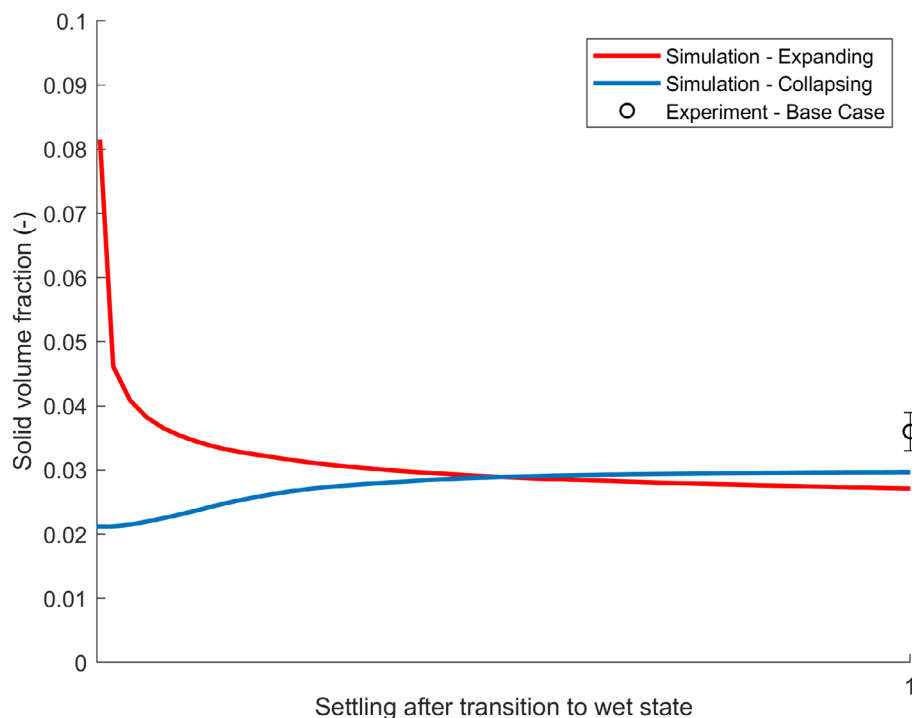
We therefore model networks with the same distribution of fiber lengths based on the measurement of a fiber length distribution from the same material as the measured sample (Figure S1 in the Supporting Information) but with varying degree of simulated compression, resulting in varying dry solid volume. We use the distribution of fibers with the fines being excluded, but account for them in terms of the solid volume fraction contribution based on the fines contributing with 8% of the total weight of fibers. We then simulate the dry-to-wet transition of networks with varying dry solid volume fraction due to varying prior compression to see if this assumption reproduces the behavior seen in our measurements reflected in the behavior of the wet solid volume fraction tending to the same value.

The simulation results formulated to explain the findings from the experimental *Base Case* (submerged and unloaded network) show two simulations of the networks with the same composition but with different dry solid volume fractions due to different prior simulated compression (Figure 2). More specifically, the change in the network solid volume fraction when turning to a wet state is assessed for networks with a starting solid volume fraction of 0.021 and 0.081, respectively. The results clearly show the solid volume fraction tending to the same value for the two networks in the wet state independent of prior dry solid volume fraction, showing a good agreement with the experimentally observed behavior of the same wet-state solid volume fraction being independent of a dry-state one (Figure 1). The terminal (or the equilibrium) solid volume fraction for the simulated networks reaches the values of 0.030 and 0.027, respectively, which is within 30% of the corresponding measured wet solid volume fraction from *Base Case* with an average value of 0.036.

To be noted when discussing the simulation results, some uncertainties exist in defining the material parameter values and conditions. For example, the cross sections of the fibers in the current numerical framework are circular, while the natural fluff pulp fibers are having a varying cross section shape, oftentimes closer to a rectangular one. Such an effect is not included in our framework.

In terms of the areal density of the network, carrying out simulations with the required number of fibers in the framework to represent the current measured material would not be feasible in terms of the computational time. At the same time, a physical network with the same low areal density as that of the numerical framework network would not be possible to manufacture in a good and controlled way. We argue here that the mentioned difference in the areal density of the network has a relatively minor impact. This is supported by our earlier work where we tested effect of compression while varying areal density up to four times the areal density used in this work showing marginal impact from areal density on SVF.⁶ If we sweep over the thickness direction of the networks, we see an edge effect close to the top of the samples where the network has a lower solid volume fraction than that of the bulk. As long as we exclude the edge-effect from the top of the samples, the solid volume fraction has very

FIGURE 2 Simulation and experimental results of the solid volume fraction of networks settling after transitioning from a dry to a wet state. The red curve shows a compressed network with a high solid volume fraction in the dry state reducing in the solid volume fraction as it settles (the expanding network). The blue curve shows an uncompressed network with a low solid volume fraction in the dry state increasing in the solid volume fraction as it settles (the collapsing network). The results show the solid volume fraction after settling in the wet state tending to the same value. The horizontal axis is the simulation timestep normalized by the number of timesteps to reach the designated stop criterion, based on first and second derivatives being below a selected threshold value.



little variation in the thickness-direction. A higher areal density, however, could affect the fiber orientation in the network when deposited, with an increased orientation in the z-direction. An estimation of the impact of varying the fiber orientation can be done using the work of Toll that gives a difference of 20% between fully 2D and 3D fiber orientations for the networks with an equivalent degree of packing in terms of the contact number.³

Related to the fiber stiffness, we have investigated its effect on the terminal network solid volume fraction. It was found to have a minor impact in the unloaded case, with a reduction of the fiber stiffness by 30% impacting the terminal solid volume fraction by less than 4%. This is explained by the very weak forces acting on the network (only gravity), which leads to very small deformations of the network even with the reduced fiber stiffness.

To further find out how the numerical simulations can explain the underlying physics, we proceed by replicating the *Case II* measurements in simulations. The simulation of *Case II* is performed by compressing the network from the wet state, after the network has reached the terminal solid volume fraction in an unloaded state. The compression is done using a top wall of 1×1 cm. The wall is moved in sequences of slow compressive movements followed by a stopping in order to let the network relax and reduce the kinetic energy. The solid volume fraction and pressure are registered after each relaxation-sequence.

The results from a simulated compression corresponding to the conditions of the *Case II* measurements are compared to the measured value in Figure 3. The simulation results show that the simulated networks are indeed mechanically stable after the dry-to-wet transition. A comparison to measurements, (Figure 3), gives a solid volume fraction of 0.092 at 0.45 kPa from the fitted line based on the van Wyk equation with the closest datapoint from the simulations

being a solid volume fraction of 0.096 at 0.53 kPa. The simulation results agree very well with the measured average solid volume fraction of 0.086 at 0.45 kPa.

The shown agreement between the simulations and measurements, both in terms of the networks with varying dry solid volume fractions transitioning to close to the same wet solid volume fraction (Figure 2), and in terms of a value of the solid volume fraction to which the wet solid volume fraction transitions (Figure 3), allows us to conclude:

- The change in the network solid volume fraction from dry to wet state can be explained as driven mainly by the disappearance of fiber–fiber adhesion in combination with changes in fiber mechanical properties when wet.
- A nonreversible deformation in the dry state, creating high solid volume fraction networks, is for the range of compressions tested in this work mainly caused by the synergetic effect of adhesion and plastic deformation at contact points.⁶
- Low-solid volume fraction-networks in a dry state are prevented mainly by adhesion from compacting to a higher solid volume fraction packing.

We now proceed with investigating the phenomena behind the independence of the wet volume fraction on the prior dry solid volume fraction and the main network and fiber parameters influencing the level of the solid volume fraction in the wet state.

4 | THEORETICAL CONSIDERATIONS

We now want to complement our experimental and numerical work with a theoretical explanation of the underlying phenomena when

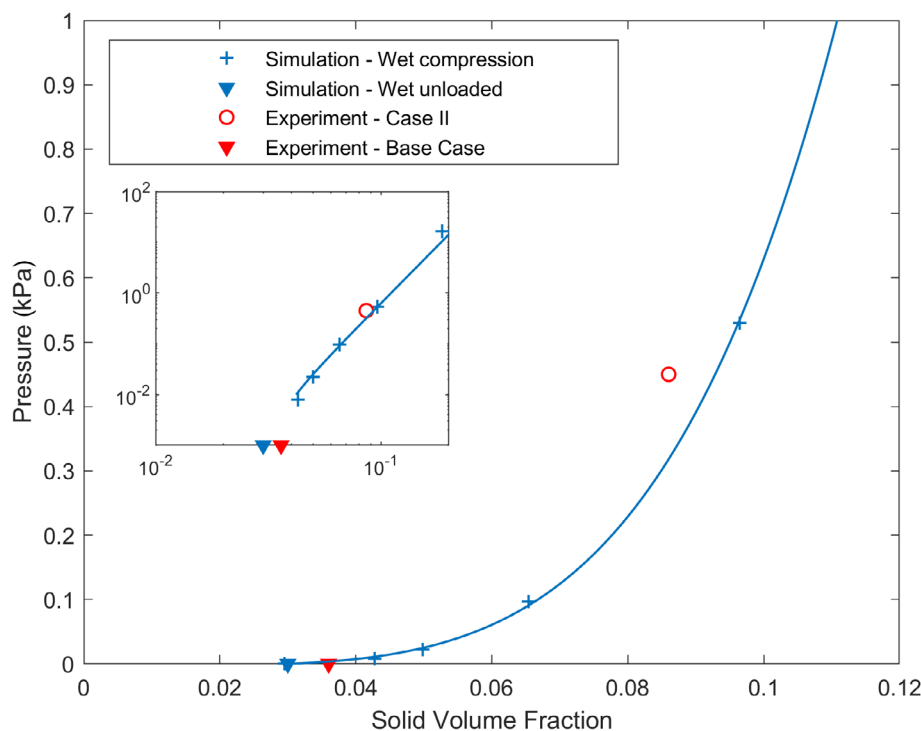


FIGURE 3 Measured solid volume fraction under 0.45 kPa (red circle) load compared to the simulated pressure vs. solid volume fraction (blue markers). The resulting solid volume fraction at 0.45 kPa shows a good agreement between the measured (0.086) and simulated values (0.09). Inset: pressure vs. solid volume fraction for the same results in a log–log scale. The fitted line based on the van Wyk equation is added to guide the eye.¹

fiber networks transition from a dry to a wet state. Based on the conclusions above, we hypothesize that uncompressed networks with a low solid volume fraction in the dry state should in the wet state, due to disappearance of adhesion, collapse to the state of *maximum unforced packing*, defined as the limiting solid volume fraction above which application of pressure resulting in deformation of fibers is required for random fiber networks in the absence of adhesion. Networks with prior compression, having a high solid volume fraction in the dry state, should on the other hand, upon disappearance of adhesion, have their constituent fibers revert to an unstrained state, while expanding the network up to the same state of *maximum unforced packing*.

Theoretical explanations for *maximum unforced packing* of networks of straight rigid rods of constant length were proposed by Evans and Gibson,⁴ Toll,³ and Wouterse et al.⁵ The explanations are based on expressions for predicting the number of fiber–fiber contacts as a function of the solid volume fraction, sometimes referred to as the random contact equation, as written by Toll³:

$$N_c = \frac{8}{\pi} \phi r f. \quad (1)$$

Here, N_c is the average number of fiber–fiber contacts, ϕ is the network solid volume fraction, r is the fiber aspect ratio, and f is a fiber orientation factor taking the value of $\pi/4$ for a 3D orientation. This is combined with the theory for mechanical stability in fiber networks as a function of the average number of fiber–fiber contacts. The theory for stability of the network is based on a local caging argument related to the *caging number*, the latter defined as the average minimum number of randomly placed fiber–fiber contacts on a single fiber that immobilize all its translations and rotations. Stable packings then

occur when a high enough fraction of fibers is immobilized by neighboring fibers leading to a stability of the entire network. We rearrange the random contact equation (Equation 1) by inserting the average number of fiber–fiber contacts to be equal to the *caging number*, γ , which yields the equation for ϕ_{\max} , maximum unforced packing³:

$$\phi_{\max} = \frac{\pi \gamma}{8 r f}. \quad (2)$$

Toll in his work with the modeling of *maximum unforced packing*, for the same type of network of straight rigid rods of constant length, used a value of 8 for the *caging number*, based on results from Evans and Gibson.^{3,4} For fibers with a high aspect ratio and a constant fiber length in the absence of adhesion, Wouterse et al. found the *caging number* of fibers to be 9 using Linear Complementarity Problem (LCP) calculations.⁵ The same authors also compared their findings to mechanical contraction simulations using molecular dynamics (MD) simulations for random packing of thin rods to determine the *stability onset*, defined as the limiting solid volume fraction upon which further contraction leads to a nonvanishing pressure. The authors found the average number of fiber–fiber contacts to be around 7.5. It is worth to highlight here the difference between the states of *maximum unforced packing* and *stability onset* of a network. Regarding the small discrepancy in the contact number between the LCP and MD simulations, Wouterse et al. note that, while *stability onset* is reached in the MD simulations, the lower value of 7.5 is “probably due to the packings being not completely jammed and further densification should be possible.” The current authors interpret this as that the states of *maximum unforced packing* and *stability onset* can be very close to each other for this type of networks in the

absence of adhesion and minor influence of friction and surface roughness. The states, however, are not the same and the range between *stability onset* and *maximum unforced packing*, ranging from 7.5 to 9 average number of fiber–fiber contacts, could represent a range where the unloaded network can be in a mechanical equilibrium.

To support the conclusions obtained by the simulations with theoretical considerations, we continue the analysis by looking at numerically obtained information on fiber contacts. The goal is to determine whether the state to which wet networks settle following our simulated dry-to-wet transition is in fact in agreement with the theoretical results for maximum unforced packing and stability onset for random packing of thin rods. We note, however, that the results from literature showing that the range of stability onset and maximum unforced packing is characterized by the average number of fiber–fiber contacts for fibers being close to the caging number were obtained for networks consisting of fibers with a constant fiber length.^{3,5} When considering that the fiber aspect ratio impacts the average number of fiber–fiber contacts at a given solid volume fraction, (Equation 1), we argue that we cannot automatically assume that the same results hold for networks consisting of fibers with varying aspect ratios. We have therefore chosen to carry out similar simulated dry-to-wet transitions as outlined above, but this time with a constant fiber length. Our objective here is to be able to make a more direct comparison with theoretical findings obtained by other research groups and find out

whether our numerical framework produces networks that indeed transition to the state of maximum unforced packing. Additionally, we will investigate the generality of conclusion 1 from the Measurements section to see whether the state to which the network transitions when going from a dry to a wet state is independent of a prior dry solid volume fraction also for networks with another composition of constituent fibers. To do so, we deposit two new networks with a constant fiber length of 0.8 mm (aspect ratio 37) and 2.0 mm (aspect ratio 93) based on the arithmetic average and length-weighted average fiber length from the measured sample in our experiments (see Section S2 and Figure S1). We then repeat simulating the transition from a dry to a wet state in the same procedure as for the network with a varying fiber length and using the same fiber properties. For each fiber length we performed one simulation with an uncompressed network having a dry solid volume fraction lower than the maximum unforced packing and one simulation with a compressed network having a dry solid volume fraction higher than the maximum unforced packing (Equation 2), in total four simulations (Figure 4).

The obtained solid volume fraction of the initially dry networks and the ones after transitioning to the wet state for the four networks show how the wet-state solid volume fraction is tending to the same level for the networks consisting of fibers with the same aspect ratio, A–B and C–D (Figure 4; specifications of cases A–D are summarized in Table S2). Such a behavior is the same as seen before for the networks with fibers of a varying fiber length (Figure 2). The form of the

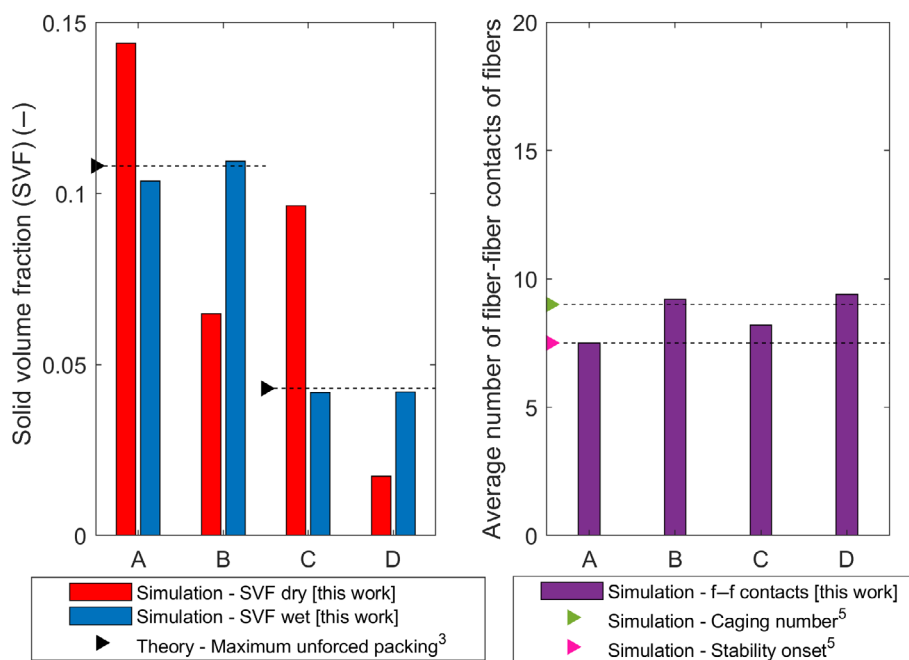


FIGURE 4 Results for four networks, A, B, C, and D (see Table S2, for case specifications), transitioning from a dry to a wet state. The left-hand graph shows the results of the solid volume fraction of an initially dry network and of the solid volume fraction of the networks after transitioning to the wet state. The results show how the wet solid volume fraction is tending to the same wet solid volume fraction for the networks consisting of fibers with the same aspect ratio, A–B and C–D. The value of the solid volume fraction to which the network is tending is dependent on the aspect ratio and agrees well with the theory for maximum unforced packing from Toll.³ The right-hand graph shows the average number of fiber–fiber (f–f) contacts after transitioning to the wet state for the same four networks. The average number of contacts is in the range of 7.5–9.5, corresponding to what is given in the simulations of caging number and stability onset by Wouterse et al.⁵

dependence of the degree of packing on the fiber aspect ratio agrees with that from the theory for *maximum unforced packing*.^{3,5} When comparing the simulated results to theoretical considerations, we use the expression for the *maximum unforced packing*, (Equation 2), with a *caging number* assumed to be 8 in Toll's work, r is the fiber aspect ratio and f is a scalar having a value of $\pi/4$ for a 3D random orientation. The simulated resulting wet solid volume fraction shows very good agreement with the calculated *maximum unforced packing*. For the fibers with an aspect ratio of 37 (A and B) results show a wet solid volume fraction of 0.104 and 0.109 compared to the theoretical value from (Equation 2) of 0.108. The corresponding values for the networks C and D (aspect ratio 93) are 0.041 and 0.042, respectively, and compare well with the theoretical value of 0.043. The close agreement seen between the simulated results and the theoretical value shows us that, in spite of the differences (e.g., in that the simulated network is loaded by its own weight and that the fibers are not rigid), our model system reverts to a state which is well predicted by topology-based theory for the state of *maximum unforced packing*. This indicates that for the networks with fiber mechanical properties of wet pulp fibers simulated in this work, gravity and fiber deformation due to the networks own weight plays a marginal role and that the resulting SVF is determined primarily by fiber geometry.

The simulated average number of fiber–fiber contacts (Figure 4) has a relatively constant value for all four networks in the range of 7.5–9.4, which is similar to the simulations of the *caging number* and *stability onset* by Wouterse et al.⁵ In that work, the authors obtain values of 9 and 7.5 for the average number of fiber–fiber contacts based on the LCP and MD simulations, respectively.⁵

We now go back to the results of the average number of fiber–fiber contacts (Figure 4). We see that the two expanding networks

(A and C, with a decreasing solid volume fraction) have a slightly lower average number of contacts (7.5 and 8.2, respectively), while the two collapsing networks (B and D, with an increasing solid volume fraction) have a slightly higher average number of contacts (9.2 and 9.4, respectively). This small difference between the two types of networks can probably be explained by the transient nature of the simulated systems. We argue that despite having reached a stable value in terms of the solid volume fraction, the systems are not in a state of a zero kinetic energy, something that could slightly affect the network on the level of fiber–fiber contacts. It is possible that in the collapsing networks, with the fibers colliding with each other as they settle, the number of fiber–fiber contacts is slightly over-estimated due to the residual kinetic energy. Conversely, in the expanding networks, with the fibers pushing away each other as the network settles, the number of fiber–fiber contacts is slightly under-estimated, again due to the residual kinetic energy in the system.

If we wish to further investigate the simulation results replicating *Base case* measurements in terms of fiber–fiber contacts, we cannot directly apply the theory of average number of fiber–fiber contacts reaching the *caging number* as a threshold for stability onset. The reason is that the mentioned concept has been formulated only for networks involving fibers with a constant fiber length. We look thus at the average number of fiber–fiber contacts individually for each aspect ratio of the fibers in the distribution (Figure 5). We do this by identifying the aspect ratio of the two contacting fibers for each contact in the bulk of the material and assigning the counted contacts to fibers of the corresponding fiber aspect ratios. If the entire fiber is not within the bulk of the material, which is our region of interest, the number of contacts is normalized to represent the full fiber length.

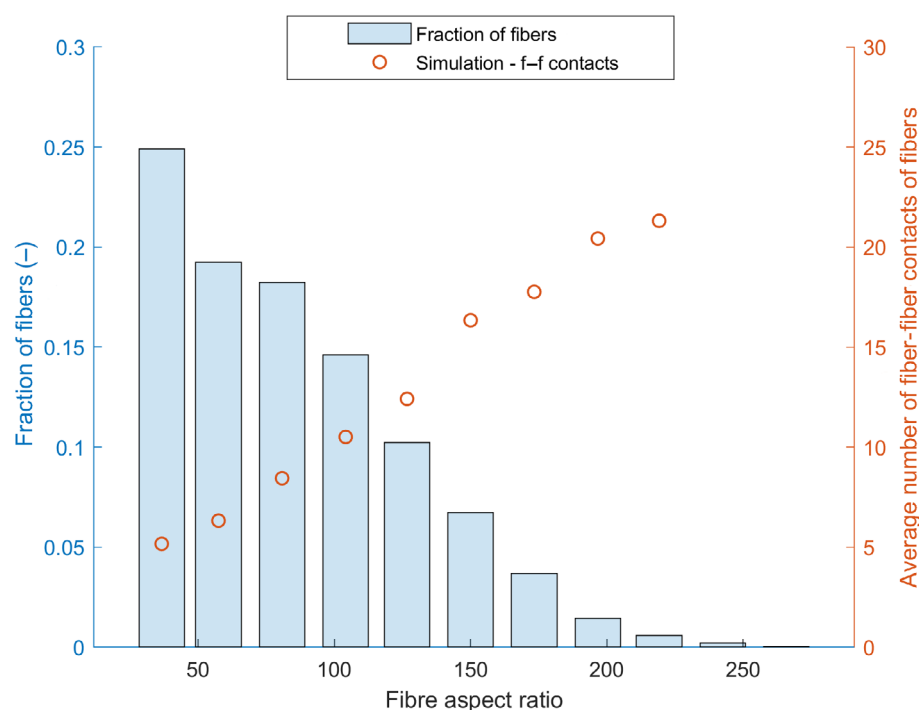


FIGURE 5 The simulated average number of fiber–fiber (f–f) contacts for networks after transitioning from a dry to a wet state and settling (circles). The fiber length distribution is added for reference (bars).

We see that the number of average contacts per fiber varies for fibers with different fiber lengths and we also observe a close to a linear relationship (Figure 5). The values for average contacts per fiber of the two longest fractions of fibers are omitted from the graph based on insufficient statistics with less than three fibers of the highest and the second highest fiber aspect ratios being part of the simulation and within the region of interest. If we instead look at the average distance between fiber–fiber contacts divided by a fiber diameter, L_c/D , we get an average distance between contacts which is almost independent of the fiber aspect ratio. This implies that the appearance of contacts along fibers is of random nature and that the probability of encountering a fiber–fiber contact per distance traveled, if traveling along a fiber, is independent of the fiber aspect ratio. This reasoning agrees with the random contact equation used by both Toll and Wouterse for networks with a constant fiber length, but also in the present case for the networks with a nonconstant fiber length. Looking at the distribution of the number of fiber–fiber contacts (Figure S4), the result shows a distribution skewed toward some fibers having very many contacts. This differs from the results of networks with a constant fiber length from Wouterse, where the distribution of contacts followed a close to normal distribution centered around the value of the *caging number*.⁵ This deviation in the results is driven by the distribution of fiber lengths in the present study with the fibers in the higher range of aspect ratios accounting for the high contact numbers.

Relating the results from the network with a distribution of fiber lengths to the theory of maximum packing, we observe that 51.2% of the fibers have 9 or more contacts as related to the value for *caging number* of 9 calculated by Wouterse.⁵ The average number of contacts of fibers is 10.7, slightly higher than the *caging number* and likely driven by the longest fibers having the number of contacts far above the *caging number*. However, there is a contrast in terms of caging of fibers between the networks with a constant fiber length as opposed to those having a fiber length distribution. For the former networks, while the average number of fiber–fiber contacts coincides with the *caging number* at the stability onset, due to the *caging number* being an average number of contacts required to cage the fiber, the results from Wouterse et al. show that essentially all the fibers in the network are caged when the network reaches the *stability onset*.⁵ The fibers with less contacts than the *caging number* are still caged due to the distribution of contacts required to cage a fiber. The results from Wouterse et al. also show that roughly 4% of fibers can be caged and blocked from rotations and translations perpendicular to the axis of symmetry with as few as five randomly placed contacts.⁵ The results from the present study, on the other hand, show that for our network with distributed fiber lengths, a significant fraction of fibers will likely be uncaged. Indications of this can be seen in Figure 5 showing over 10% of the fibers having even less than five contacts and the shortest fraction of fibers having an average number of fiber–fiber contacts around five. While fibers can still be at mechanical equilibrium, as non-straight fibers can be at equilibrium with as few as two contacts, it remains unclear how much the fraction of uncaged fibers contributes to the overall network stability.

To conclude this section, we observe that the simulated results of the fiber networks with a constant fiber length show that the state of close to constant solid volume fraction to which wet networks is tending is in fact in good agreement with the predictions from theories for *maximum unforced packing* and simulated results of stability onset for random packing of thin rods (Figure 4). Based on this, it is reasonable to conclude that the simulated results from Figure 2, using the same framework and the simulation procedure, albeit using a distribution of fiber lengths, are in fact in a state within the narrow range of stability onset and *maximum unforced packing*. Based on the previously shown very good agreement for the simulated results replicating *Base Case* and the measurements from Figure 3, together with the conclusion that the simulated results after the dry-to-wet transition settle to a mechanically stable state within the narrow range of *stability onset* and *maximum unforced packing*, we conclude that:

- The state to which pulp fiber networks settle after the dry-to-wet transition in an unloaded case is a mechanically stable state within the narrow range of *stability onset* and *maximum unforced packing*.
- The value of the solid volume fraction to which the networks are tending is determined primarily by the aspect ratio of the constituent fibers.

5 | CONCLUSIONS

In this article, we provide a comprehensive experimental, numerical, and theoretical explanation of the change in the solid volume fraction and mechanical response for nonbonded pulp fiber networks transitioning from a dry to a wet state.

We have first experimentally characterized and quantified the change in a softwood fluff pulp network structure when transitioning from a dry to a wet state. From this part, we conclude that:

- For the range of compressions tested in this work, the state to which the network transitions when going from a dry to a wet state is independent of its prior dry solid volume fraction.
- The value of the solid volume fraction of networks in the wet state is extremely sensitive to the degree of loading of the network.
- No fiber or network parameter which affects final packing of the wet sample has been affected by the compression of the network or the effect is annulled by the presence of water.

Afterward, we have compared experimental results with our simulation results using a DEM framework to identify fundamental phenomena behind the observed changes in the network solid volume fraction due to the transition. The results show very good agreement between the two types of studies, both in terms of the networks with different initial dry solid volume fractions tending to close to the same wet solid volume fraction and in terms of the value of the solid volume fraction to which the wet solid volume fraction is tending in the unloaded case, as well as under a slight load. This allows us to conclude that:

- Dry nonreversible deformation, creating high solid volume fraction networks, is for the range of compressions tested in this work mainly caused by the synergetic effect of adhesion and plastic deformation in contact points.⁶
- Low-solid volume fraction-networks in a dry state are prevented from compacting to a higher solid volume fraction packing mainly by adhesion.
- The change in the network solid volume fraction from dry to wet state can be explained as primarily driven by the disappearance of fiber–fiber adhesion in combination with changes in fiber mechanical properties when wet.

Finally, we have combined our simulation results and the analyses performed by other research groups to provide a theoretical explanation regarding the network state to which a wet network transitions. Based on the demonstrated very good agreement between the simulated results and the measurements from the unloaded network in *Base Case* (Figure 3), together with the conclusion that the simulated networks transition to a mechanically stable state within the narrow range of *stability onset* and *maximum unforced packing* (Figure 4), we are able to conclude that:

- The state to which pulp fiber networks are settling after the dry-to-wet transition in an unloaded case is a mechanically stable state within the narrow range of *stability onset* and *maximum unforced packing*.
- The level of the solid volume fraction to which the networks are tending after the dry-to-wet transition is determined primarily by the aspect ratio of the constituent fibers.

These results bring important new knowledge on the changes in the solid volume fraction for natural nonbonded fluff pulp networks with an inherent distribution in fiber lengths when going from a dry to a wet state. This type of network is used in a large range of common hygiene products designed for absorption of liquids. The findings in this work will be highly beneficial for the development of such products since crucial parameters for product function such as permeability and capillary pressure are directly dependent on the solid volume fraction and how the solid volume fraction transitions from a dry to a wet state.

AUTHOR CONTRIBUTIONS

Per Bergström: Conceptualization (equal); data curation (equal); formal analysis (equal); investigation (equal); methodology (equal); software (equal); validation (equal); visualization (equal); writing – original draft (equal). **Charlotta Hanson:** Conceptualization (equal); formal analysis (equal); investigation (equal); methodology (equal); supervision (equal); writing – review and editing (equal). **Henrik Ström:** Conceptualization (equal); formal analysis (equal); investigation (equal); methodology (equal); project administration (equal); supervision (equal); writing – review and editing (equal). **Srdjan Sasic:**

Conceptualization (equal); formal analysis (equal); investigation (equal); methodology (equal); project administration (equal); supervision (equal); writing – review and editing (equal).

DATA AVAILABILITY STATEMENT

The numerical data from Figures 1–5 as well as Figures S1 and S4 are tabulated in the Supporting Information.

ORCID

Per Bergström  <https://orcid.org/0000-0003-3463-0249>

Henrik Ström  <https://orcid.org/0000-0002-8581-5174>

REFERENCES

1. Van Wyk C. 20—note on the compressibility of wool. *J Text Inst Trans.* 1946;37(12):T285–T292.
2. Komori T, Makishima K. Numbers of fiber-to-fiber contacts in general fiber assemblies. *Text Res J.* 1977;47(1):13–17.
3. Toll S. Packing mechanics of fiber reinforcements. *Polym Eng Sci.* 1998;38(8):1337–1350.
4. Evans K, Gibson A. Prediction of the maximum packing fraction achievable in randomly oriented short-fibre composites. *Compos Sci Technol.* 1986;25(2):149–162.
5. Wouterse A, Luding S, Philipse AP. On contact numbers in random rod packings. *Granul Matter.* 2009;11(3):169–177.
6. Bergström P, Hanson C, Ström H, Sasic S. Uniaxial compression of fibre networks—the synergetic effect of adhesion and elastoplasticity on non-reversible deformation. *Powder Technol.* 2022;395:301–313.
7. Buchholz FL, Pesce SR, Powell CL. Deswelling stresses and reduced swelling of superabsorbent polymer in composites of fiber and superabsorbent polymers. *J Appl Polym Sci.* 2005;98(6):2493–2507.
8. Lorbach C, Fischer WJ, Gregorova A, Hirn U, Bauer W. Pulp fiber bending stiffness in wet and dry state measured from moment of inertia and modulus of elasticity. *BioResources.* 2014;9(3):5511–5528.
9. EDANA. EDANA Standard Procedure NWSP 120.6.R0. https://www.edana.org/docs/default-source/international-standards/table-of-content-nw-standard-procedures-20210105.pdf?sfvrsn=4ede1add_20
10. Kloss C, Goniva C, Hager A, Amberger S, Pirker S. Models, algorithms and validation for open-source DEM and CFD–DEM. *Prog Comput Fluid Dyn.* 2012;12(2–3):140–152.
11. Richter C. Liggghts-with-bonds. GitHub Repository. <https://github.com/richti83/LIGGGHTS-WITH-BONDS> 2015.
12. Schramm M, Tekeste MZ, Plouffe C, Harby D. Estimating bond damping and bond Young's modulus for a flexible wheat straw discrete element method model. *Biosyst Eng.* 2019;186:349–355.

SUPPORTING INFORMATION

Additional supporting information can be found online in the Supporting Information section at the end of this article.

How to cite this article: Bergström P, Hanson C, Ström H, Sasic S. The dry-to-wet transition of fiber networks—Return to mechanical stability. *AIChE J.* 2023;e18148. doi:10.1002/aic.18148